In Vivo Imaging Reveals Rapid Astrocyte Depletion and Axon Damage in a Model of Neuromyelitis Optica-Related Pathology

Marina Herwerth, MD,[1,2,3] Sudhakar Reddy Kalluri, MSc,[1] Rajneesh Srivastava, MSc,[1] Tatjana Kleele, PhD,[2] Selin Kenet, MSc,[2] Zsolt Illes, MD, PhD,[4,5] Doron Merkler, MD,[6,7,8] Jeffrey L. Bennett, MD, PhD,[9] Thomas Misgeld, MD,[2,3,10,11,12] and Bernhard Hemmer, MD[1,3,12]

Objective: Neuromyelitis optica (NMO) is an autoimmune disease of the central nervous system, which resembles multiple sclerosis (MS). NMO differs from MS, however, in the distribution and histology of neuroinflammatory lesions and shows a more aggressive clinical course. Moreover, the majority of NMO patients carry immunoglobulin G autoantibodies against aquaporin-4 (AQP4), an astrocytic water channel. Antibodies against AQP4 can damage astrocytes by complement, but NMO histopathology also shows demyelination, and—importantly—axon injury, which may determine permanent deficits following NMO relapses. The dynamics of astrocyte injury in NMO and the mechanisms by which toxicity spreads to axons are not understood.
Methods: Here, we establish in vivo imaging of the spinal cord, one of the main sites of NMO pathology, as a powerful tool to study the formation of experimental NMO-related lesions caused by human AQP4 antibodies in mice.
Results: We found that human AQP4 antibodies caused acute astrocyte depletion with initial oligodendrocyte survival. Within 2 hours of antibody application, we observed secondary axon injury in the form of progressive swellings. Astrocyte toxicity and axon damage were dependent on AQP4 antibody titer and complement, specifically C1q.
Interpretation: In vivo imaging of the spinal cord reveals the swift development of NMO-related acute axon injury after AQP4 antibody-mediated astrocyte depletion. This approach will be useful in studying the mechanisms underlying the spread of NMO pathology beyond astrocytes, as well as in evaluating potential neuroprotective interventions.

ANN NEUROL 2016;79:794–805

Axon damage is a common phenomenon in many neurological diseases, including those of neuroimmunological origin.[1] Indeed, in multiple sclerosis (MS), the degree of axon damage is an important determinant of chronic disability.[2,3] However, because the pathological cascades that drive axon damage in MS are not known, only limited understanding of the mechanisms underlying this important aspect of pathology has been possible. In contrast, in neuromyelitis optica (NMO), an autoimmune disease that mainly affects the optic nerve and spinal cord,[4] the autoimmune target has been identified in the majority of patients. Most NMO patients have a

View this article online at wileyonlinelibrary.com. DOI: 10.1002/ana.24630

Received Oct 27, 2015, and in revised form Mar 2, 2016. Accepted for publication Mar 3, 2016.

Address correspondence to Dr. Bernhard Hemmer or Dr. Thomas Misgeld, Technical University of Munich, Munich, Germany. E-mail: hemmer@tum.de or thomas.misgeld@tum.de

From the [1]Department of Neurology, Klinikum rechts der Isar, Technical University of Munich, Munich, Germany; [2]Institute of Neuronal Cell Biology, Technical University of Munich, Munich, Germany; [3]Munich Cluster for Systems Neurology (SyNergy), Munich, Germany; [4]Department of Neurology, Division of Clinical and Experimental Neuroimmunology, University of Pecs, Pecs, Hungary; [5]Department of Neurology and Institute of Clinical Research, Odense University Hospital, University of Southern Denmark, Odense, Denmark; [6]Department of Pathology and Immunology, University of Geneva, Geneva, Switzerland; [7]Division of Clinical Pathology, Geneva University Hospital, Geneva, Switzerland; [8]Department of Neuropathology, University Medical Center, Göttingen, Germany; [9]Departments of Neurology and Ophthalmology, Program in Neuroscience, University of Colorado Denver School of Medicine, Aurora, CO; [10]German Center for Neurodegenerative Diseases (DZNE), Munich, Germany; [11]Center of Integrated Protein Science (CIPSM), Munich, Germany; and [12]equal contributing senior authors

Additional supporting information can be found in the online version of this article

794 © 2016 The Authors. Annals of Neurology published by Wiley Periodicals, Inc. on behalf of American Neurological Association. This is an open access article under the terms of the Creative Commons Attribution-NonCommercial-NoDerivs License, which permits use and distribution in any medium, provided the original work is properly cited, the use is non-commercial and no modifications or adaptations are made.

specific serum antibody response to aquaporin-4 (AQP4),[5–8] a water channel, which in the central nervous system (CNS) is expressed on astrocytes, especially on perivascular and superficial glia limitans processes. Antibodies to AQP4 (AQP4-Ig [immunoglobulin]) are also present in the cerebrospinal fluid (CSF) of NMO patients, although at a lower titer.[8–10] Occurrence of AQP4-Ig in serum and CSF, loss of astrocytes, deposition of complement, and infiltration of macrophages in NMO lesions together imply a specific immune response against AQP4-expressing astrocytes.[11–13] Indeed, intraperitoneal injection of NMO serum immunoglobulins containing AQP4-Ig or of AQP4-specific recombinant antibodies combined with opening of the blood–brain barrier (BBB) by T-cell-mediated inflammation or intracerebral needle injury can produce astrocyte loss and demyelination in rats.[9,13–15] Similarly, injection of AQP4-Ig and human complement into mouse brain induces NMO-like lesions.[16] The majority of AQP4-Ig belongs to the IgG_1 subclass, which can activate the complement cascade upon target binding,[8] and hence the presence of complement and antibody effector function is essential in transfer models that show astrocyte loss. In line with these observations, plasma exchange, which reduces circulating IgG and complement levels, is effective in treating NMO relapses.[17] In addition to astrocyte loss and immunopathology, demyelination and axon damage have been identified histologically in NMO.[18,19] Although demyelination has been investigated in some detail in previously reported animal models, the impact of AQP4-Ig-mediated astrocyte loss on axons has received less attention.[9,13–16] This is despite the fact that axon damage appears to be an early feature of human pathology[19] and likely underlies some of the residual deficits after NMO relapses. Thus, improved models to study the mechanisms by which AQP4-Ig-induced damage spreads from astrocytes to axons are needed.

Here, we use an in vivo two-photon imaging approach to the mouse spinal cord that we previously established[20–22] to gain insight into AQP4-Ig-mediated lesion formation. We found that AQP4-Ig-containing samples obtained from NMO patients (as well as a recombinant AQP4-IgG from a clonotypic plasma blast present in the CSF of an NMO patient) caused acute, dose-dependent and (human) complement-mediated loss of astrocytes when applied at the pial surface of the spinal cord at IgG concentrations found intrathecally in NMO.[23] Using combinatorial transgenic labeling of different CNS cell types, we revealed secondary axon damage, which, in onset and extent, correlated with astrocyte loss and AQP4-IgG titer. This imaging approach will provide a novel way to study, in real time and with single-cell resolution, how secondary damage emerges after AQP4-Ig-mediated astrocyte loss in nascent NMO-like spinal lesions.

Materials and Methods

Animals

We used 2- to 4-month-old transgenic male and female mice to visualize astrocytes (*Aldh1l1*:GFP; obtained from MMRRC: strain Tg(Aldh1l1-EGFP)OFC789Gsat/Mmucd[24]) and axonal morphology (*Thy1*:OFP[25] courtesy of Jeff Lichtman, Harvard University, Cambridge, MA) for in vivo experiments and 3- to 5-week-old *Aldh1h1*:GFP mice for ex vivo experiments. In some experiments 2- to 4-month-old C57BL/6 mice were used as transgene-free controls. *Plp*:CreER × *ROSA*:STOP-TdTomato mice (Ai14; The Jackson Laboratory, Bar Harbor, ME)[26,27], in which oligodendrocytes are labeled, were used to control for cell-type specificity (tamoxifen injection proved unnecessary because of constitutive activity of the CreER in adult animals). Tissue samples from AQP4 knockout mice were obtained from Alan Verkman (University of California San Francisco, San Francisco, CA).[28] Animal experiments were conducted in accord with local regulations and were approved by the responsible regulatory agencies.

Patients, Serum/Plasma Samples, and Complement Sources

NMO patients were recruited from the Department of Neurology, University of Pecs, (Pecs, Hungary) and from the Department of Neurology, Klinikum rechts der Isar, Technical University of Munich (Munich, Germany). All patients were examined by neurologists specialized in neuroimmunology and fulfilled the diagnostic criteria for NMO based on Wingerchuk's criteria.[4] Serum or plasma samples of 4 AQP4-Ig-positive individuals were included in this study, 3 of which (referred to as NMO1-3 below) were used in in vivo experiments. As controls, samples of 3 healthy subjects (ctrl1-3, below), without signs of an autoimmune disease or infection at the time of blood sampling, were included in cooperation with the blood bank of the Bavarian Red Cross. Blood samples were collected by venipuncture, centrifuged at 3,000rpm for 10 minutes, split into aliquots, frozen for storage at –80 °C, and thawed only on the day of the experiment. All blood samples were tested for being human immunodeficiency virus, hepatitis B virus, and hepatitis C virus negative. All subjects gave written informed consent to the use of their blood samples for research. Moreover, for complement depletion and reconstitution assays, we obtained human C1q-depleted sera and purified C1q component from Merck Millipore (Billerica, MA).

Acute Brain Slice Preparation

Ex vivo acute brain slice experiments were performed as previously described.[29] In brief, brains from *Aldh1l1*:GFP mice were removed, cut centrally into coronal slices (300 µm) in Ringer's/artificial cerebrospinal fluid (aCSF; pH 7.4 at 4 °C) containing (in mM): 125 NaCl, 26 $NaHCO_3$, 2.5 KCl, 1.25 NaH_2PO_4, 2 $CaCl_2$, 1 $MgCl_2$, and 20 glucose, followed by recovery at 35 °C

for 1 hour. Slices were transferred to a recording chamber and continuously superfused with 50ml of recirculating, heated (30 °C), and oxygenated (95% O_2/5% CO_2) aCSF (1.5–2.0ml/min). After complement inactivation at 56 °C for 30 minutes, we applied diluted NMO or control sera/plasma (IgG levels adjusted to the values indicated in the figures), together with 4% non-heat-inactivated serum from healthy donors (HDs) as a source of complement (referred to as HD serum below), which remained in the aCSF from 0 to 180 minutes of the experiment. Image stacks (~30 images, 2-μm z-spacing) were acquired using a two-photon microscope (Olympus FV1000 MPE tuned to 910 nm, equipped with a ×25/1.05 numerical aperture [N.A.] water dipping cone objective; Olympus, Tokyo, Japan) at 3-minute intervals for 3 hours.

Surgical Procedures and In Vivo Imaging

Laminectomy surgeries were performed as previously described[21]: Mice were anesthetized by an intraperitoneal injection of ketamine-xylazine (87mg/kg/13mg/kg, respectively) or meditomidin 0.5mg/kg, midazolam 5mg/kg, and fentanyl 0.05mg/kg. Anesthesia was reapplied as needed (every 60–120 minutes). After a double dorsal laminectomy over the fourth lumbar, L4, and L5 segments, mice were suspended using compact spinal cord clamps.[30] A well around the opening was built using 2-4% agarose to hold aCSF (as above, glucose omitted or alternatively, in mM: 148.2 NaCl, 3.0 KCl, 0.8 Na_2HPO_4, 0.2 NaH_2PO_4, 1.4 $CaCl_2$, and 0.8 $MgCl_2$). An imaging window free from dura was established in the imaging area using a bent hypodermic needle. In some experiments, astrocyte death was verified by addition of ethidium homodimer-1 (1:500, 0.56mg/ml stock; Invitrogen, Carlsbad, CA).

In vivo imaging of the lumbar spinal cord was performed as previously described.[21,31] Briefly, stacks were acquired using two-photon microscopes (Olympus FV1000 MPE or FVMPE-RS tuned to 910 nm for green fluorescent protein [GFP] alone and 980nm for GFP/OFP [orange fluorescent protein], equipped with a ×25/1.05 N.A. water-dipping cone objective). All light was first filtered through a 690 nm short-pass dichroic mirror. Fluorescence was collected using a G/R filter set (BA 495-540, BA 570-625) mounted in front of gallium arsenide phosphide photomultiplier tubes. Time-lapse stacks were acquired at 3-minute intervals for 3 hours (astrocyte loss) or at 15-minute intervals for 6 hours (axon damage) with the following parameters: 35 images (zoom 1.8–2.0; pixel size: 0.28–0.38 μm) with 1-μm z-step. Diluted heat-inactivated serum/plasma was applied every 30 minutes, supplemented with 20% of non-heat-inactivated HD serum as a complement source. Compared to experiments with acute brain slices, a higher concentration was needed, most likely because of restricted penetration and possibly the presence of complement blockers in vivo. Serum/plasma was present in the spinal opening for the initial 90 minutes of the experiment, after which it was replaced with aCSF (at 90 minutes and renewed every 60 minutes until the end of the experiment). Transient delivery of the NMO sample and complement source was designed to induce an acute, well-defined injury and reduce consumption of sparse patient-samples. In a set of control experiments using NMO1 samples and HD serum for up to 8 hours continuously, we found no qualitative difference between prolonged and transient applications, although, as expected, astrocyte depletion and the degree of axon swellings was more pronounced after longer exposure to patient IgG and complement. To confirm AQP4 specificity, we also performed experiments using a human IgG_1 recombinant antibody rAb 7-5-53 reconstructed from a clonotypic plasma blast obtained from the CSF of an NMO patient (r-AQP4-IgG)[9]. r-AQP4-IgG was applied at 1.5 μg/ml of IgG supplemented with 20% of non-heat-inactivated HD serum. The rAb ICOS-5-2, a divalent human IgG_1 antibody of unknown specificity, developed from a chronic meningitis patient, served as an isotype control (r-ctrl-IgG).

We have previously demonstrated that phototoxicity does not appear to have a measurable impact on the health of spinal axons under such imaging conditions.[21,22,31,32] Moreover, histological analysis confirmed NMO serum-/plasma-mediated astrocyte loss in the absence of oligodendrocyte loss in superficial spinal cord layers when no imaging was done (see below and *cf.* Fig 1G,H). Additionally, axonal pathology could be confirmed in experiments in which only an initial and a final image (at 6 hours) were taken (*cf.* Fig 4B). To rule out a spurious influence of the transgenic labeling of axons, we performed experiments without imaging using wild-type (C57BL/6) and transgenic animals and antitubulin staining (see below). The analysis was performed by a scorer blind to the treatment conditions and genotypes and showed a comparable percentage of axonal swellings in spinal cords treated with NMO serum/plasma irrespective of genotype (data not shown).

Immunohistochemistry and Histological Analysis

After transcardiac perfusion with 4% paraformaldehyde (PFA) in 0.01M of phosphate-buffered saline (1×PBS; in mM: 1.5 KH_2PO_4, 2.7 KCl, 8.1 Na_2HPO_4, and 137 NaCl), the spinal cord and brain from *Adh1l1*:GFP mice were postfixed for 24 hours in 4% PFA, then dissected and put in sucrose (30%) solution for a further 12 to 24 hours. Subsequently, 20-μm-thick cryosections were cut in a cryostat. For staining, NMO1 plasma or serum (and control sera from healthy donors) was used at 1:1,000 in 0.2% Triton X-100, 10% normal goat serum, and 1% bovine serum albumin in 1×PBS (followed by incubation with appropriate secondary antibodies; antihuman IgG 1:200, ABC-complex, streptavidin Alexa Fluor 555 1:1,000). Glial fibrillary acidic protein (GFAP) antibody (rat; Invitrogen) was used at a concentration of 1:200 (followed by goat Alexa Fluor 647–conjugated antirat IgG 1:1,000). Sections were mounted in 4′,6-diamidino-2-phenylindole (DAPI)-containing mounting medium, and image stacks were recorded on a confocal microscope (Olympus FV1000) equipped with × 20/0.8 N.A. and ×60/1.42 N.A. oil-immersion objectives. For tubulin stainings, we used an Alexa Fluor 647–conjugated antibody to tubulin III beta (mouse; BioLegend) at 1:200 and stained spinal cord whole mounts[22] of wild-type control (C57BL/6) or *Thy1*:OFP mice that were either treated with NMO or control samples plus HD serum for 6 hours without

imaging. Confocal images were taken as described above for GFAP stainings. To control for effects of imaging and transgene expression on astrocyte loss, we performed dorsal laminectomy surgery on wild-type control (C57BL/6) and *Aldh1l1*:GFP mice as described for imaging above. We applied heat-inactivated NMO, as well as control samples with HD serum as a complement source as detailed above, but no imaging was performed. Instead, after 3 hours, animals were perfused, their spinal cords embedded in paraffin, and subjected to histopathological analysis according to standardized protocols as described previously.[33] Briefly, immunostaining was performed using the following primary antibodies: rabbit/anti-GFAP (astrocytes; 1:2,000; code no.: Z0334; Dako, Carpinteria, CA) and mouse/anti-NogoA (mAb11C7, 1:20,000; kindly provided by M.E. Schwab, Zurich, Switzerland). Bound primary antibodies were visualized using a ready-to-use, peroxidase-based secondary detection system (EnVision; Dako) with 3,3′-diaminobenzidine as chromogen (hemalaun counterstaining of nuclei). Immunostained sections were scanned using a Panoramic Digital Slide Scanner 250 FLASH II (3DHISTECH Ltd., Budapest, Hungary) at 200 × magnification. Astrocyte and oligodendrocyte densities in the superficial dorsal spinal cord (<50 μm from pial surface) were counted manually using Panoramic Viewer software (3DHISTECH Ltd.) by a scorer blind to the treatment conditions and genotypes.

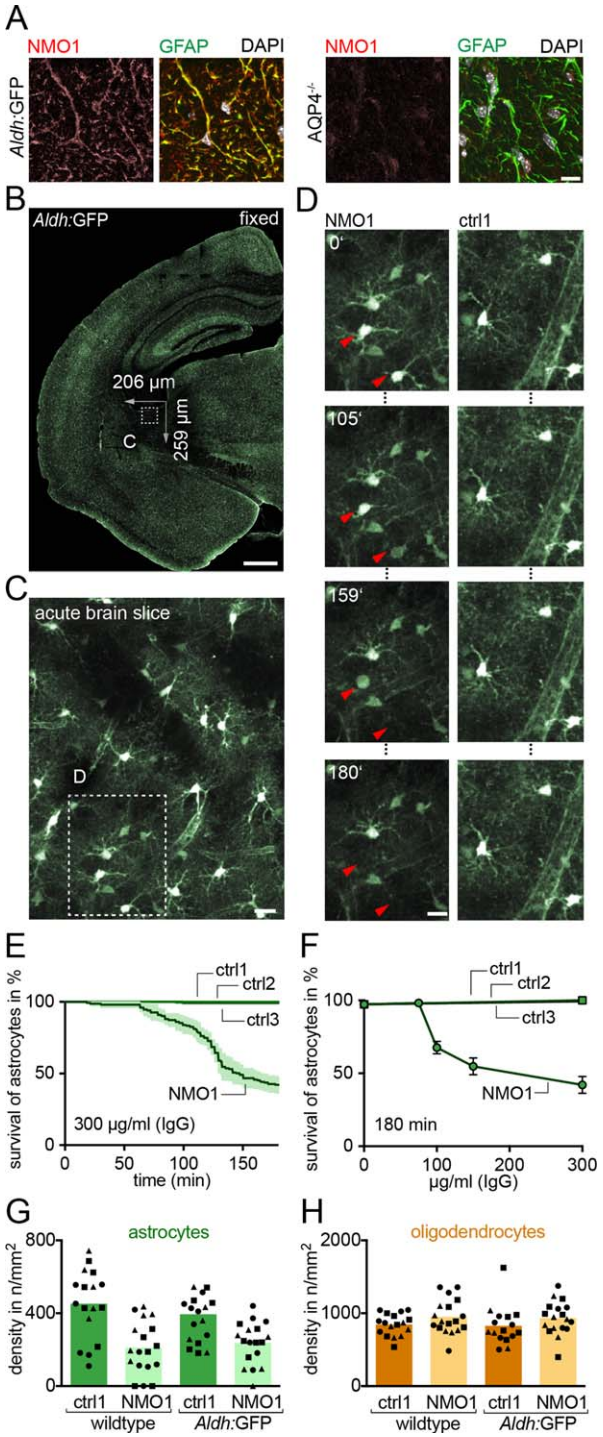

FIGURE 1: NMO patient-derived samples contain AQP4-Ig that stains and ablates mouse astrocytes in vitro and in vivo. (A) White matter spinal cord cryosections of *Aldh1l1*:GFP mice (*Aldh*:GFP, left; GFP not shown) and AQP4-knockout-mice (AQP4$^{-/-}$, right), stained for astrocytes (GFAP, green), nuclei (DAPI, white), and with an AQP4-Ig-containing NMO sample (NMO1, red). (B) Confocal image of a fixed brain slice from an Aldh1l1-GFP mouse. Box indicates the relative size of a typical time-lapse area as magnified in (C). (C) Two-photon image of astrocytes in an acute brain slice. Boxed area time-lapsed in (D), left column. (D) Time-lapse images taken from acute brain slices every 3 minutes for 3 hours, showing astrocytes (red arrowheads) that lose fluorescence and die in the presence of a heat-inactivated AQP4-Ig-containing NMO sample (NMO1) and HD serum as a source of complement. A control serum (ctrl1) had no detectable effect under the same conditions. (E) Astrocyte survival over 180 minutes in acute brain slices in the presence of control sera from healthy subjects (ctrl1-3) and an AQP4-Ig-containing NMO serum (NMO1, 300 μg/ml of IgG; n = 3 recordings for each sample; $p < 0.0001$, log-rank test). (F) Dose-response curve of astrocyte survival after 180 minutes for an AQP4-IgG containing NMO (NMO1) and three control samples (n = 3 recordings for each sample; $p = 0.0045$, Mann–Whitney *U* test, NMO1 vs pooled ctrl1-3 for 300-μg/ml IgG concentration). HD serum (4%) as a source of complement was present in all recordings in (E) and (F). (G and H) Histopathological quantification of astrocyte (GFAP; G) and oligodendrocyte (Nogo-A; H) densities in the superficial spinal cord of wild-type and *Aldh1l1*:GFP mice after 180-minute in vivo application of heat-inactivated AQP4-Ig-containing NMO (NMO1) or a control sample (ctrl1) supplemented with HD serum into a laminectomy opening (n = 3 mice for each genotype/treatment combination; GFAP: wild-type ctrl1 vs NMO1 $p < 0.001$; Aldh:GFP ctrl1 vs NMO1 $p < 0.01$; Nogo-A: no significant differences, D'Agostino and Pearson's normality test, followed by analysis of variance and Holm-Sidak's multiple comparisons test). Scale bars, 10 μm in (A), 500 μm in (B), 20 μm in (C), and 10 μm in (D). Data are presented as mean ± standard error of the mean. AQP4 = aquaporin-4; DAPI = 4′,6-diamidino-2-phenylindole; GFAP = glial fibrillary acidic protein; GFP = green fluorescent protein; HD = healthy donor; Ig = immunoglobulin; NMO = neuromyelitis optica.

AQP4-Specific Immunoglobulin Depletion From Patient Samples

HEK293 cells (~2*10^9) expressing C-terminally His-tagged AQP4 were lysed in 5ml of nondenaturing base lysis buffer (in mM: NaCl 300, Tris-HCl [pH 7.4] 10, phosphate buffer [pH 7.4] 50, imidazol [pH 7.4] 10, 200 µl of ethylenedimainetetraacetic acid [EDTA]-free protease inhibitor cocktail, and 5 µl of benzoase) with 1% decyl β-D-maltopyranoside for 40 minutes at room temperature. Lysate was centrifuged at 50,000*g* and cleared supernatant incubated with 500 µl of pre-equilibrated HisPur Cobalt Resin (Life Technologies, Carlsbad, CA) for 1 hours. The resin was spun down and washed thoroughly with washing buffer I (as above, but containing only 0.01% decyl β-D-maltopyranoside) multiple times until absorption at 280nm became undetectable. Resin was resuspended in 40ml of 0.03% H_2O_2 and agitated at room temperature for 2 hours for oxidation of Co(II) to Co(III), spun down, and washed with wash buffer II (PBS and 100mM of EDTA) to strip away any unoxidized divalent ions.[34] This AQP4 resin was used to deplete antigen-specific Ig from samples. Control columns were prepared in the same way, however, using sham-transfected HEK293 cells. For access to sufficient volumes, AQP4-specific Ig depletion experiments were performed with NMO1 plasma.

AQP4-Antibody Titration Assay

Sera and recombinant Abs were measured at different dilutions using a cell-based flow cytometry assay. The human glioblastoma cell line, LN18, was stably transduced using a lentiviral vector to overexpress human AQP4-M23 as previously reported (LN18^{AQP4}).[8,9] Results were expressed as median fluorescence

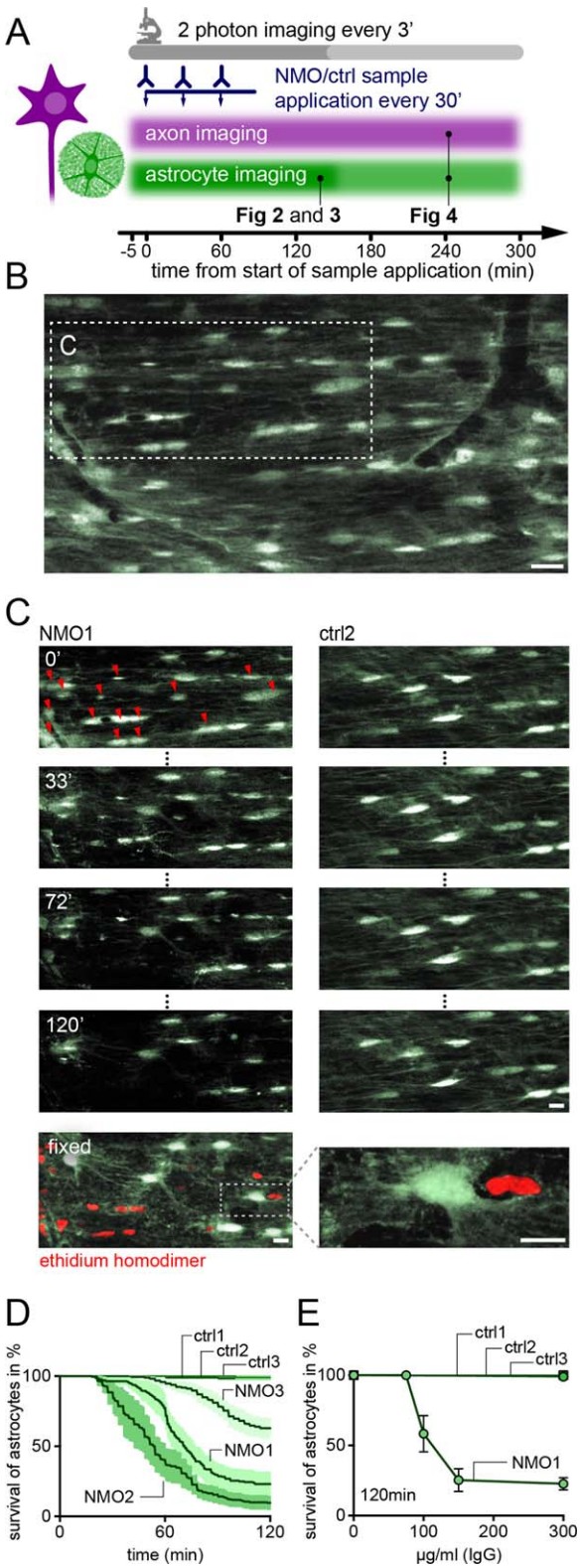

FIGURE 2: Human AQP4-Ig samples induce rapid astrocyte pathology in the murine spinal cord in vivo. (A) Schematic sketch of the setup of the in vivo imaging experiment. Note that NMO and control samples were exchanged three times and replaced by aCSF after 90 minutes. (B) Overview of a typical imaging area in *Aldh1l1*:GFP mice (GFP, green) before application of NMO samples. Boxed area is followed by time lapse in (C), left column. (C) In vivo time-lapse series of astrocytes (GFP, green) that lose fluorescence and die (red arrows) in the presence of a heat-inactivated AQP4-Ig-containing NMO sample (NMO1) plus HD serum as complement source. Control serum (ctrl2) does not affect astrocytes under the same conditions. Bottom panel shows uptake of the cell death marker, ethidium homodimer (red), which was present during the in vivo recording, in astrocytes that lost fluorescence in response to AQP4-Ig-containing serum (boxed area is magnified to the right). (D) Percentage of surviving astrocytes in the presence (0–90 minutes) of control (ctrl) and AQP4-Ig-containing NMO samples (NMO) with HD serum as complement source (n = 3–5 recordings per sample; $p < 0.001$, for NMO1-3 each tested vs ctrl1, log-rank test; adjusted to 150 µg/ml for NMO and 300 µg/ml for ctrl samples). (E) Dose response of astrocyte loss as a function of total IgG concentration after 120 minutes for one NMO and several control samples (n = 3–5 recordings per sample, 100–300 µg/ml; n = 1–2 recordings for 0–75 µg/ml). All samples were complemented with the same amount of HD serum ($p = 0.0045$, for NMO1 vs pooled ctrl1-3 for 300-µg/ml concentration, Mann–Whitney *U* test). Scale bars, 20 µm in (B), 10 µm in (C). Data are presented as mean ± standard error of the mean. aCSF = artificial cerebrospinal fluid; AQP4 = aquaporin-4; GFAP = glial fibrillary acidic protein; GFP = green fluorescent protein; HD = healthy donor; Ig = immunoglobulin; NMO = neuromyelitis optica.

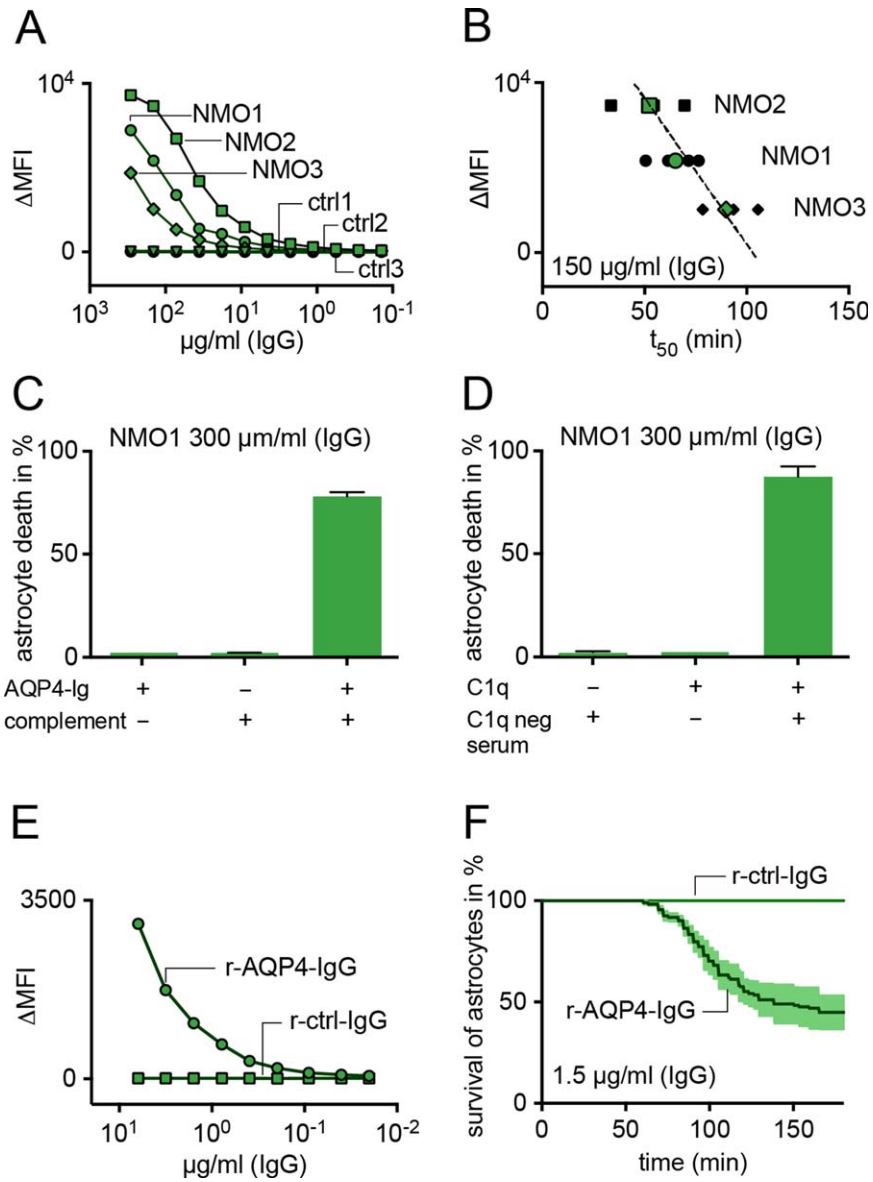

FIGURE 3: NMO-related astrocyte pathology is AQP4-Ig specific and complement dependent. (A) Titration of the NMO patient-derived sera and control sera in an in vitro binding assay. Antibody titers in serum correspond to the difference in binding to an AQP4-transduced cell line and a control cell line (delta median fluorescence intensity; ΔMFI). (B) Correlation between the AQP4-Ig titer and the time when 50% astrocyte loss was reached (t_{50}; 150 µg/ml). Mean values are presented as green data symbols. (C) Complement inactivation (complement –) or AQP4-Ig depletion by an AQP4-preabsorption column (AQP4 Ig–) abolishes the pathological effects on astrocytes caused by the AQP4-Ig-containing NMO1 sample. A preabsorption column without AQP4-antigen has no effect (AQP4 IgG+; n = 2–5 for all conditions; $p < 0.0001$, log-rank test). (D) C1q factor depletion (C1q neg serum+/C1q–) abolishes the pathological effects on astrocytes caused by the NMO1 sample. Resubstitution of purified C1q factor (20 µg/ml) reinstates the effect (C1q neg serum+/C1q+), whereas C1q alone has no effect (C1q neg serum–/C1q+; n = 3 for all conditions; $p < 0.0001$, log-rank test). (E) Titration as in (A) of a recombinant AQP4 antibody (r-AQP4-IgG) and of a control antibody (r-ctrl-IgG). (F) Percent of surviving astrocytes in the presence of r-AQP4-IgG and r-ctrl-IgG (1.5 µg/ml; n ≥ 3 recordings for all conditions, $p < 0.0001$, log-rank test). Data are presented as mean ± standard error of the mean. AQP4 = aquaporin-4; HD = healthy donor; Ig = immunoglobulin; NMO = neuromyelitis optica.

intensities (MFI) corrected for background binding to a cell line that was transduced with an empty vector ($LN18^{CTR}$). Samples were considered to be positive if the ΔMFI value was above 50 (where ΔMFI is the MFI difference between $LN18^{AQP4}$ and $LN18^{CTR}$, and a measure of the concentration of AQP4-specific IgG).

Image Processing and Data Analysis

Images were processed using the open-source image analysis software, Fiji[35] and Adobe Creative Suite. Gamma was adjusted linearly in all figure panels; gamma was adjusted nonlinearly in video files to enhance visibility of morphological detail. Percentage of cell loss was defined as percentage of cells that lost >50% of their fluorescence, which was accompanied by clear

changes in morphology (rounding, process blebbing). Axon morphology in a neuroinflammatory setting was staged as described previously.[21,22] Only axons that were observable across all time points during the experiment over at least 50 μm were analyzed. Each axonal swelling was verified by observations of morphology within unprocessed three-dimensional (3D) image stacks. We relinquished scoring the morphological changes of astrocytes and axons blindly, given that the difference between control and NMO experiments was obvious. Data sets were processed with Excel (Microsoft Corporation, Redmond, WA). For survival curves (Figs 1E, 2D, 3F, and 4C,G), a custom-written Python script was used for analysis.

Statistical Analyses

The proportion of surviving astrocytes and of axons with swellings was analyzed with Kaplan-Meier estimates, and treatment differences were compared with log-rank test. For control experiments (axon damage without time lapse), we used non-parametric tests. For comparison of two conditions, we used the Mann–Whitney *U* test; for comparison of more than two conditions, we used Kruskal-Wallis' followed by Dunn's multiple comparison test. For histopathology, normal distribution of values obtained from individual analyzed fields of view was confirmed using D'Agostino and Pearson's normality test, followed by analysis of variance and Holm-Sidak's multiple comparisons test. Data are shown as mean ± standard error of the mean (SEM); significance statements are included in the figure legends.

Results

NMO Patient-Derived AQP4 Antibodies Induce Acute Astrocyte Pathology Ex Vivo

As a first step toward establishing an in vivo assay for NMO-related neuropathology, we used isolated mouse brain tissue to (1) confirm that human AQP4-Ig can bind and damage mouse astrocytes, as shown previously in slice cultures,[36] (2) define the time course, concentration ranges, and complement requirements that characterize these effects, and (3) devise a transgene-based readout of astrocyte death, taking advantage of astrocyte-

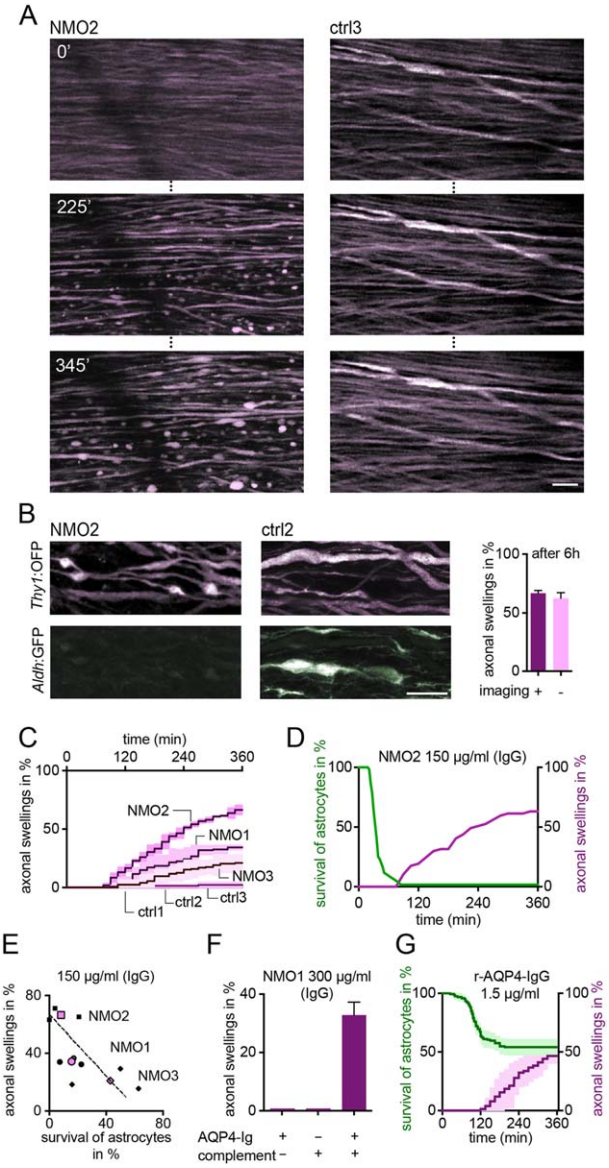

FIGURE 4: AQP4-antibody mediated astrocyte loss is followed by axonal pathology in vivo. (A) Time-lapse imaging of the spinal cord in vivo (every 15 minutes for 6 hours) reveals axons that develop progressive swellings in the presence of an AQP4-Ig-containing sample (NMO2), whereas in the presence of a control sample (ctrl3), axons remain unaffected. (B) The same experiment as in (A), but without two-photon imaging. Afterward, the tissue was fixed and images of the spinal cord were taken on a confocal microscope (axons, magenta; astrocytes, green) and quantitatively compared to imaged samples (same data as in C), as shown in the graph on the right (n = 3; $p = 0.7$, Mann–Whitney *U* test). (C) Percentage of swollen axons as a function of time using three different NMO patient-derived AQP4-Ig-containing samples (NMO1-3; 150 μg/ml) vs three control samples (ctrl1-3; 300 μg/ml, n > 120 axons from three experiments for each sample; $p < 0.0001$, log-rank test of NMO1-3 individually vs ctrl1). (D) Example of concomitant quantification of astrocyte survival (green) and axonal swellings (magenta) in one recording using sample NMO2 complemented with HD serum, which were present from 0 to 90 minutes. (E) Correlation between survival of astrocytes and axonal swellings after 6 hours induced by the indicated AQP4-Ig-containing samples. Mean values are presented as magenta data symbols. (F) Analogous to Figure 3C, complement inactivation and AQP4-Ig depletion abolish the pathological effects of NMO patient-derived samples on axons (n = 2–3 for each condition; $p < 0.0001$, log-rank test; 360 minutes). (G) Percentage of astrocyte survival (green) and axonal swellings (magenta) in the presence of the recombinant AQP4-antibody ('r-AQP4-IgG'; 1.5 μg/ml, n > 125 axons, n = 3; $p < 0.0001$ compared to r-ctrl-IgG, data not shown, log-rank test). Scale bars, 10 μm in A and B. Data are presented as mean ± standard error of the mean. AQP4 = aquaporin-4; HD = healthy donor; Ig = immunoglobulin; NMO = neuromyelitis optica; OFP = orange fluorescent protein.

specific GFP expression in *Aldh1l1*:GFP mice.[24] First, we confirmed that our AQP4-Ig-containing NMO samples specifically labeled GFAP-positive astrocytes in mouse spinal cord white matter. This staining was absent on tissue of AQP4-knockout mice (Fig 1A) and when we used AQP4-Ig-negative serum samples (data not shown). Second, we applied diluted, heat-inactivated, AQP4-Ig-positive NMO (or AQP4-Ig-negative control) samples together with a complement source (non-heat-inactivated HD serum) to acute brain slices from *Aldh1l1*:GFP mice. Within 60 minutes, we observed swelling and fragmentation of astrocyte processes, as well as rounding of cell somata, followed by loss of fluorescence (Fig 1B–D, Supplementary Video 1). The degree of astrocyte loss was dose dependent and patient specific (survival of astrocytes after 180 minutes as mean percentage ± SEM, average of 3 experiments each: 42.1 ± 5.8 and 63.9 ± 7.3 for two different AQP4-Ig-positive NMO samples, one of which [NMO1] is illustrated in Fig 1E,F). In contrast, control sera had no effects over our observation period of 3 hours (100.0 ± 0.0, 99.4 ± 0.6,and 99.6 ± 0.4 for three control sera and three repeats each) — moreover, in subsequent experiments, we found the toxic effects of these NMO samples to be specifically mediated by AQP4-Ig and the classical complement cascade (see below). Together, these experiments confirmed the notion that NMO patient-derived AQP4-Ig induce astrocyte pathology, which we could follow dynamically using *Aldh1l1*:GFP mice.

Human AQP4 Antibodies Exert Acute Pathological Effects in Mouse Spinal Cord In Vivo

To establish an in vivo model of NMO-related astrocyte toxicity, we first confirmed that a quasi-intrathecal route of application (application into a laminectomy with dura removal) would suffice to induce astrocyte pathology. We chose this approach because it is compatible with the in vivo imaging technique we sought to employ, which depends on a surgical exposure of the dorsal spinal cord, but also because NMO patients can harbor substantial amounts of AQP4-Ig in their CSF (as well as plasma blasts that secrete such antibodies).[8–10,23] To determine astrocyte pathology in this setting, we performed standard histopathological analysis after a 3-hour treatment with an AQP4-Ig-positive NMO sample plus HD serum applied to a laminectomy. We found a clear reduction in GFAP staining in the superficial spinal cord. At the same time, an oligodendrocyte marker remained unchanged, confirming astrocyte-specific toxicity of AQP4-Ig-containing NMO samples in the presence of complement (Fig 1G,H) as shown previously for intraparenchymal injections.[16]

Next, we took advantage of a two-photon imaging approach to visualize cells in the dorsal spinal cord of anesthetized mice.[21,32] After establishing a spinal cord imaging window in *Aldh1l1*:GFP mice, we applied heat-inactivated AQP4-Ig-positive NMO samples (n = 3; NMO1 to NMO3) together with untreated HD serum as a source of complement from 0 to 90 minutes (after which antibodies and complement were replaced by aCSF; the same HD serum at a fixed concentration of 20% was used in all in vivo experiments). This allowed us to follow AQP4-Ig-mediated astrocyte toxicity over several hours (Fig 2A). In line with our ex vivo observations, we found that NMO patient-derived AQP4-Ig-containing samples caused swelling and fragmentation of astrocytes in vivo, followed by loss of fluorescence, which correlated with uptake of the cell-death marker dye, ethidium homodimer (Fig 2B,C; Supplementary Video 2). Astrocyte damage was dose dependent and correlated with the AQP4-Ig titer measured in an in vitro binding assay (Figs 2D,E and 3A,B; mean survival of astrocytes ± SEM after 120 minutes at 150 μg/ml in %: NMO1 23.0 ± 8.6, n = 5; NMO2 9.7 ± 4.7, n = 4; NMO3 62.9 ± 7.3, n = 5; t_{50} in min: NMO1 65.1 ± 4.5; NMO2 52.3 ± 7.4; NMO3 89.9 ± 5.1). In the presence of control sera with untreated HD serum astrocytes remained unaffected even at high concentration (300 μg/ml of IgG; mean survival of astrocytes ± SEM after 120 minutes in %: ctrl1 99.1 ± 0.9, n = 3; ctrl2 100.0 ± 0.0, n = 3; ctrl3 98.5 ± 0.8, n = 3). Moreover, for the first hour after application, AQP4-Ig-induced cell death appeared to be astrocyte specific. When we performed the same experiments with genetically labeled oligodendrocytes (*Plp*:CreER × *ROSA*:STOP-TdTomato), we observed no overt loss of fluorescence during a 3-hour imaging period, even though some oligodendrocyte somata assumed a more rounded shape (mean survival of oligodendrocytes ± SEM after NMO1 application at 150 μg/ml after 120 minutes in %: 97.0 ± 3.0, n = 3).

NMO-Related Astrocyte Toxicity Is AQP4 Specific and Complement Dependent

To further elucidate the characteristics of NMO-related astrocyte toxicity in our model, we selectively depleted AQP4-Ig from one NMO sample (plasma sample NMO1) using an AQP4-preabsorption column, which abolished astrocyte damage (Fig 3C). A preabsorption column without AQP4 antigen had no effect (mean astrocyte death ± SEM in %: 0.7 ± 0.5, n = 5 vs 78.1 ± 2.1, n = 3 after preabsorption with and without AQP4 on column, respectively; 360 minutes, Ig adjusted

to 300 μg/ml in both conditions). Complement inactivation (i.e., heat treatment of the HD serum added with the patient samples) also abrogated astrocyte toxicity (Fig 3C, mean astrocyte death ± SEM in %: 0.0 ± 0.0, n = 2; 360 minutes), confirming that AQP4-Ig-mediated astrocyte toxicity is a two-component system requiring AQP4-Ig and complement.[16,36] To elucidate which complement activation pathway mediates the observed astrocyte damage, we used (1) C1q-depleted complement, (2) C1q factor alone, and (3) C1q-reconstituted complement in the presence of AQP4-Ig-containing NMO samples. We found that whereas C1q depletion alone protected astrocytes, toxicity was re-established by C1q-reconstitution (Fig 3D; C1q depletion: 1.8 ± 1.0, n = 3; C1q alone: 0.0 ± 0.0, n = 3; C1q reconstitution: 87.5 ± 5.0, n = 3; 180 minutes; all values mean ± SEM). This implies that our model depends on the classical complement pathway.

To rule out the possibility that the observed effect was influenced by other antibodies or non-specific factors present in patient samples, we took advantage of the recombinant AQP4-specific antibody 7-5-53 (r-AQP4-IgG), which was generated from a clonotypic plasma blast present in the CSF of an NMO patient.[9] When combined with a human complement source, a low concentration of r-AQP4-IgG (1.5 μg/ml) induced robust astrocyte pathology (Fig 3E,F; mean survival of astrocytes ± SEM after 120 minutes in %: 44.9 ± 8.5 vs 100.0 ± 0.0 for r-AQP4-IgG vs r-ctrl-IgG, respectively; n = 3 in both conditions).

NMO-Related Astrocyte Toxicity Leads to Axonal Pathology

Our in vivo model provides a unique opportunity to investigate whether NMO-related astrocyte toxicity affects surrounding axons, given that axon damage can be followed by two-photon imaging in great detail.[21,22] We used combinatorial transgenic labeling of astrocytes and axons (*Aldh1l1*:GFP × *Thy1*:OFP double transgenic mice) and followed changes in axons for up to 6 hours after application of NMO samples (Figs 2A and 4A, Supplementary Video 3). With this labeling, we observed widespread secondary axon damage in the form of progressive swellings, which formed along the length of many axons starting at 100–120 minutes after NMO sample application until the end of our 6-hour observation period (i.e., well beyond the time during which we applied NMO samples, which was discontinued after 90 minutes). This axon pathology was not the consequence of phototoxicity, given that the same percentage of swollen axons was noted, whether or not a time-lapse series was acquired (Fig 4B). Axonal swellings occurred after astrocyte loss was well advanced, and the percentage of swollen axons corresponded to the AQP4-Ig titer and hence the degree of astrocyte loss (Fig 4C–E; *cf.* Fig 3A). After application of control sera, even at high concentrations, no change of axonal morphology could be observed (Fig 4A,C; mean percentage of axonal swellings ± SEM after 360 minutes: NMO1, 34.3 ± 2.1; NMO2, 66.5 ± 4.1; NMO3, 21.1 ± 7.2 vs with ctrl1, 2.3 ± 2.4; ctrl2, 0.0 ± 0.0, ctrl3, 1.5 ± 1.3; n = 3 for all conditions; 150 μg/ml IgG for NMO, 300 μg/ml for ctrl samples). Notably, we did not observe axon fragmentation, which we previously demonstrated in other models of autoimmunity[21] or after blunt trauma.[22] Indeed, even after prolonged exposure to AQP4-Ig (NMO1) and HD for 8 hours (mean percentage astrocyte death ± SEM: 98.8 ± 0.6; mean percentage of axonal swellings ± SEM: 65.7 ± 6.7; n = 3), axons remained apparently continuous (Supplementary Video 4). Inactivation of the complement source or AQP4-Ig depletion from NMO samples abolished the effect on axons, suggesting that axonal pathology depends on AQP4-mediated astrocyte toxicity (Fig 4F; complement inactivation: 0.0 ± 0.0, n = 2; AQP4-immunoglobulin depletion: 0.0 ± 0.0, n = 3 vs. preabsorption column without AQP4-antigen: 32.8 ± 4.5, n = 3; all values mean ± s.e.m.). Performing the same experiments with recombinant AQP4-antibodies confirmed that r-AQP4-IgG in the presence of complement is sufficient to induce the observed secondary axonal changes with a similar relation to astrocyte damage as observed with AQP4-Ig-containing samples (Fig 4G; axon swellings in %: r-AQP4-IgG: 46.7 ± 6.3 vs r-ctrl-IgG 0.0 ± 0.0; n = 3 for each condition; all values mean ± SEM).

Discussion

Here, we use in vivo spinal imaging to reveal the temporal progression of NMO-related spinal cord pathology induced by AQP4-Ig and provide new insights into how antibody-mediated astrocyte damage affects nonastrocytic structures in the spinal cord. Astrocyte toxicity was specific to AQP4-Ig, correlated with antibody titer, and was mediated by the classical complement pathway. Our study extends previous reports on the potency of human AQP4-IgG to induce NMO-related astrocyte pathology in rodents,[9,13,14,16] while at the same time providing a unique dynamic view of astrocyte injury. Moreover, using combinatorial labeling, we found that after AQP4-Ig-induced astrocyte loss, axons rapidly developed progressive swellings. Although axonal changes in NMO lesions in the spinal cord have been described in autopsies[11,12,19] and histopathological evidence of axonal injury was found 12 hours after injection of NMO serum in mouse

brain,[16] to our knowledge, this is the first study to directly monitor the development of acute (on the order of hours) axonal pathology in an experimental NMO-related animal model. Notably, axon damage in this NMO-related model showed some unique features. Similar to experimental autoimmune encephalomyelitis (EAE), a widely used rodent model of MS, axons exposed to AQP4-IgG and complement developed early focal swellings. In EAE, however, swollen axons are often severed,[21] an irreversible form of damage commonly observed after blunt trauma.[22] Such axonal transections were not evident in our NMO-related model, at least during the first 8 hours, suggesting that there could be potential for reversing axonal damage early in an NMO lesion, as has been observed previously in other models of neuronal damage.[21,22,37,38] In addition to revealing new aspects of axon injury, our in vivo model also allows investigating the propagation of injury across the glial-neuronal network starting from a well-defined initial lesion to astrocytes. In contrast, in other neuroinflammatory models such as EAE, damage results from a complex and protracted immune insult involving both the innate and adaptive immune systems, where cellular and humoral components operate in parallel to injure multiple CNS targets. In addition, the co-visualizing myelin and oligodendrocytes with astrocytes and axons in vivo[21,31] will allow us to dissect the temporal sequence and inter-relatedness of the mechanisms governing NMO and other autoantibody-mediated CNS pathologies.

What is the mechanism driving the rapid axonal changes? Based on our experience,[21,22,32] use of recombinant reagents, and detailed controls, neither additional components in human samples, imaging, or transgenic labeling can account for the axonal swellings (for details, see Materials and Methods). Although we cannot exclude a possible direct "by-stander" attack of activated complement factors or an indirect effect by another cell type,[39] the timing, lack of associated pathology, and localization of the axonal changes make these unlikely, and suggest that axonal swelling is the consequence of astrocyte loss. Indeed, this is not entirely surprising,[40–42] given that numerous vital interactions between astrocytes and axons have been documented[43–46]: For example, astrocytes are known to scavenge glutamate,[47] and excitotoxicity has been implicated in axonal pathology during neuroinflammation.[48–50] This, together with the well-established role of excitotoxicity after hypoxia,[43,51] warrants future investigation in our NMO-related model using in vivo real-time optical techniques,[52] calcium sensors,[22,53] and selective pharmacological inhibitors. Alternatively, astrocyte loss could also reduce metabolic support for axons,[46,54–56] impair oxidative defense,[40,57–59] or alter ion and water homeostasis,[60] predisposing axons to swelling.[61] Optical monitoring of these injury mechanisms within our novel NMO model system will provide a powerful means to understand the processes underlying axon damage that emerges secondary to astrocyte loss.

Despite many advantages, our NMO-related model has a number of limitations. For instance, the poor intrinsic activity of complement and the presence of inhibitors of the classical activation pathway in mice[62] require the use of human complement with NMO samples similar to previous experimental models.[9,13,15,16] Whereas we could control for this additional cause of variability by dissociating the source of AQP4-Ig and of human complement, natural NMO lesions would use endogenous complement and hence may have different kinetics or a distinct spectrum of injury than observed in our model. Similarly, the direct application of AQP4-Ig onto a large area of exposed pial surface does not match the widely assumed primary entry route of serum AQP4-Ig by a disrupted BBB.[5] Nevertheless, the concentration of serum antibodies that we applied to the spinal cord is not outside the range of levels found in NMO patients, especially during relapses.[23] Moreover, plasma blasts and plasma cells can be present in the CSF of NMO patients and locally release AQP4-Ig,[9,63] suggesting that even in this respect our approach is compatible with some of the access routes of AQP4-Ig in human NMO.

In conclusion, we report here that human NMO-derived AQP4-Ig applied to the spinal cord in vivo can reproduce important features of NMO lesion formation, which can be monitored by in vivo imaging. Our results confirm that astrocyte loss appears to be the primary event of AQP4-Ig-induced lesion formation and rapidly results in axonal pathology. Our new approach can shed light on the interdependence of astrocyte health and axon survival in white matter tracts and potentially define a window of opportunity for neuroprotective interventions in NMO.

Acknowledgment

M.H. was supported by a grant (KKF) from Klinikum rechts der Isar of the Technical University of Munich. B.H.'s laboratory is supported by grants from the Deutsche Forschungsgemeinschaft (DFG; Transregio 128) and the German Federal Ministry of Research and Education (BMBF; Competence Network Multiple Sclerosis). T.M. is supported by the DFG Center for Integrated Protein Science (Munich, EXC 114), the European Research Council under the European Union's Seventh Framework Program (FP/2007-2013; ERC Grant Agreement no.: 616791), the German Center for Neurodegenerative

Disease (DZNE), DFG Priority Program 1710, and the DFG Collaborative Research Center 870. B.H. and T.M. are supported by the DFG-funded Munich Center for Systems Neurology (SyNergy; EXC 1010). D.M. holds a stipendiary professorship of the Swiss National Science Foundation (no. PP00P3_152928) and is supported by the Klaus-Tschira Foundation, Gebert-Rüf Foundation, and by the Swiss MS Society. J.L.B. was supported by grants from the National Institutes of Health (EY022936), the Guthy-Jackson Foundation, and the National MS Society.

We thank Manuela Budak, Nebahat Budak, and Sebahat Taskin for animal husbandry and Yvonne Hufnagel, Kristina Wullimann, Carina Nowak, Verena Grummel, and Andreas Winkler for technical assistance. We thank Prof Thomas Korn for providing AQP4 knockout mouse tissue, Prof Jeff Lichtman for sharing *Thy1*:OFP mice, and Benedikt Herwerth for help with Python scripting. We thank Leanne Godinho for comments on the manuscript. The mouse strain used for this project (STOCK Tg(Aldh1l1-EGFP)OFC789Gsat/Mmucd; identification no.: 011015-UCD) was obtained from the Mutant Mouse Regional Resource Center, a NCRR-NIH–funded strain repository, and was donated to the MMRRC by the NINDS funded GENSAT BAC transgenic project.

Author Contributions

M.H., T.M., and B.H. are responsible for concept and study design. M.H., S.K., T.K., D.M., S.R.K., R.S., J.L.B., and Z.I. were involved in sample/data acquisition and analysis; M.H., J.L.B., T.M., and B.H. drafted the manuscript and figures, with input from all the authors. T.M. and B.H. contributed equally as senior authors.

Potential Conflicts of Interest

Nothing to report.

References

1. Coleman MP, Perry VH. Axon pathology in neurological disease: a neglected therapeutic target. Trends Neurosci 2002;25:532–537.
2. Trapp BD, Peterson J, Ransohoff RM, et al. Axonal transection in the lesions of multiple sclerosis. N Engl J Med 1998;338:278–285.
3. Schirmer L, Antel JP, Brück W, Stadelmann C. Axonal loss and neurofilament phosphorylation changes accompany lesion development and clinical progression in multiple sclerosis. Brain Pathol 2011;21:428–440.
4. Wingerchuk DM, Lennon VA, Lucchinetti CF, et al. The spectrum of neuromyelitis optica. Lancet Neurol 2007;6:805–815.
5. Lennon VA, Wingerchuk DM, Kryzer TJ, et al. A serum autoantibody marker of neuromyelitis optica: distinction from multiple sclerosis. Lancet 2004;364:2106–2112.
6. Lennon VA, Kryzer TJ, Pittock SJ, et al. IgG marker of optic-spinal multiple sclerosis binds to the aquaporin-4 water channel. J Exp Med 2005;202:473–477.
7. Paul F, Jarius S, Aktas O, et al. Antibody to aquaporin 4 in the diagnosis of neuromyelitis optica. PLoS Med 2007;4:e133.
8. Kalluri SR, Illes Z, Srivastava R, et al. Quantification and functional characterization of antibodies to native aquaporin 4 in neuromyelitis optica. Arch Neurol 2010;67:1201–1208.
9. Bennett JL, Lam C, Kalluri SR, et al. Intrathecal pathogenic anti-aquaporin-4 antibodies in early neuromyelitis optica. Ann Neurol 2009;66:617–629.
10. Jarius S, Wildemann B. AQP4 antibodies in neuromyelitis optica: diagnostic and pathogenetic relevance. Nat Rev Neurol 2010;6:383–392.
11. Misu T, Fujihara K, Kakita A, et al. Loss of aquaporin 4 in lesions of neuromyelitis optica: distinction from multiple sclerosis. Brain 2007;130(pt 5):1224–1234.
12. Roemer SF, Parisi JE, Lennon VA, et al. Pattern-specific loss of aquaporin-4 immunoreactivity distinguishes neuromyelitis optica from multiple sclerosis. Brain 2007;130:1194–1205.
13. Wrzos C, Winkler A, Metz I, et al. Early loss of oligodendrocytes in human and experimental neuromyelitis optica lesions. Acta Neuropathol 2014;127:523–538.
14. Bradl M, Misu T, Takahashi T, et al. Neuromyelitis optica: pathogenicity of patient immunoglobulin in vivo. Ann Neurol 2009;66:630–643.
15. Asavapanumas N, Verkman AS. Neuromyelitis optica pathology in rats following intraperitoneal injection of NMO-IgG and intracerebral needle injury. Acta Neuropathol Commun 2014;2:48.
16. Saadoun S, Waters P, Bell BA, et al. Intra-cerebral injection of neuromyelitis optica immunoglobulin G and human complement produces neuromyelitis optica lesions in mice. Brain 2010;133(pt 2):349–361.
17. Keegan M, Pineda AA, McClelland RL, et al. Plasma exchange for severe attacks of CNS demyelination: predictors of response. Neurology 2002;58:143–146.
18. Lucchinetti CF, Mandler RN, McGavern D, et al. A role for humoral mechanisms in the pathogenesis of Devic's neuromyelitis optica. Brain 2002;125(pt 7):1450–1461.
19. Misu T, Höftberger R, Fujihara K, et al. Presence of six different lesion types suggests diverse mechanisms of tissue injury in neuromyelitis optica. Acta Neuropathol 2013;125:815–827.
20. Kerschensteiner M, Schwab ME, Lichtman JW, Misgeld T. In vivo imaging of axonal degeneration and regeneration in the injured spinal cord. Nat Med 2005;11:572–577.
21. Nikić I, Merkler D, Sorbara C, et al. A reversible form of axon damage in experimental autoimmune encephalomyelitis and multiple sclerosis. Nat Med 2011;17:495–499.
22. Williams PR, Marincu BN, Sorbara CD, et al. A recoverable state of axon injury persists for hours after spinal cord contusion in vivo. Nat Commun 2014;5:5683.
23. Jarius S, Paul F, Franciotta D, et al. Cerebrospinal fluid findings in aquaporin-4 antibody positive neuromyelitis optica: results from 211 lumbar punctures. J Neurol Sci 2011;306:82–90.
24. Yang Y, Vidensky S, Jin L, et al. Molecular comparison of GLT1 + and ALDH1L1 + astrocytes in vivo in astroglial reporter mice. Glia 2010;59:200–207.
25. Brill MS, Lichtman JW, Thompson W, et al. Spatial constraints dictate glial territories at murine neuromuscular junctions. J Cell Biol 2011;195:293–305.
26. Doerflinger NH, Macklin WB, Popko B. Inducible site-specific recombination in myelinating cells. Genesis 2003;35:63–72.
27. Madisen L, Zwingman TA, Sunkin SM, et al. A robust and high-throughput Cre reporting and characterization system for the whole mouse brain. Nat Neurosci 2010;13:133–140.

28. Ma T, Yang B, Gillespie A, et al. Generation and phenotype of a transgenic knockout mouse lacking the mercurial-insensitive water channel aquaporin-4. J Clin Invest 1997;100:957–962.

29. Herwerth M, Jensen V, Novak M, et al. D4 dopamine receptors modulate NR2B NMDA receptors and LTP in stratum oriens of hippocampal CA1. Cereb Cortex 2012;22:1786–1798.

30. Davalos D, Lee JK, Smith WB, et al. Stable in vivo imaging of densely populated glia, axons and blood vessels in the mouse spinal cord using two-photon microscopy. J Neurosci Methods 2008;169:1–7.

31. Romanelli E, Sorbara CD, Nikic IN, et al. Cellular, subcellular and functional in vivo labeling of the spinal cord using vital dyes. Nat Protoc 2013;8:481–490.

32. Sorbara CD, Wagner NE, Ladwig A, et al. Pervasive axonal transport deficits in multiple sclerosis models. Neuron 2014;84:1183–1190.

33. Steinbach K, Merkler D. Neuropathological techniques to investigate CNS pathology in experimental autoimmune encephalomyelitis (EAE). Methods Mol Biol 2016;1304:189–209.

34. Hale JE. Irreversible, oriented immobilization of antibodies to cobalt-iminodiacetate resin for use as immunoaffinity media. Anal Biochem 1995;231:46–49.

35. Schindelin J, Arganda-Carreras I, Frise E, et al. Fiji: an open-source platform for biological-image analysis. Nat Methods 2012; 9:676–682.

36. Zhang H, Bennett JL, Verkman AS. Ex vivo spinal cord slice model of neuromyelitis optica reveals novel immunopathogenic mechanisms. Ann Neurol 2011;70:943–954.

37. Li P, Murphy TH. Two-photon imaging during prolonged middle cerebral artery occlusion in mice reveals recovery of dendritic structure after reperfusion. J Neurosci 2008;28:11970–11979.

38. Eikermann-Haerter K, Arbel-Ornath M, Yalcin N, et al. Abnormal synaptic Ca2 + homeostasis and morphology in cortical neurons of familial hemiplegic migraine type 1 mutant mice. Ann Neurol 2015;78:193–210.

39. Marignier R, Nicolle A, Watrin C, et al. Oligodendrocytes are damaged by neuromyelitis optica immunoglobulin G via astrocyte injury. Brain 2010;133:2578–2591.

40. Schreiner B, Romanelli E, Liberski P, et al. Astrocyte depletion impairs redox homeostasis and triggers neuronal loss in the adult CNS. Cell Rep 2015;12:1377–1384.

41. Delaney CL, Brenner M, Messing A. Conditional ablation of cerebellar astrocytes in postnatal transgenic mice. J Neurosci 1996;16: 6908–6918.

42. Bush TG, Puvanachandra N, Horner CH, et al. Leukocyte infiltration, neuronal degeneration, and neurite outgrowth after ablation of scar-forming, reactive astrocytes in adult transgenic mice. Neuron 1999;23:297–308.

43. Fern RF, Matute C, Stys PK. White matter injury: ischemic and nonischemic. Glia 2014;62:1780–1789.

44. Cambron M, D'Haeseleer M, Laureys G, et al. White-matter astrocytes, axonal energy metabolism, and axonal degeneration in multiple sclerosis. J Cereb Blood Flow Metab 2012;32:413–424.

45. Nave KA. Myelination and support of axonal integrity by glia. Nature 2010;468:244–252.

46. Nave KA, Trapp BD. Axon-glial signaling and the glial support of axon function. Annu Rev Neurosci 2008;31:535–561.

47. Anderson CM, Swanson RA. Astrocyte glutamate transport: review of properties, regulation, and physiological functions. Glia 2000; 32:1–14.

48. Pitt D, Werner P, Raine CS. Glutamate excitotoxicity in a model of multiple sclerosis. Nat Med 2000;6:67–70.

49. Newcombe J, Uddin A, Dove R, et al. Glutamate receptor expression in multiple sclerosis lesions. Brain Pathol 2008;18:52–61.

50. Smith T, Groom A, Zhu B, Turski L. Autoimmune encephalomyelitis ameliorated by AMPA antagonists. Nat Med 2000;6:62–66.

51. Stys PK. General mechanisms of axonal damage and its prevention. J Neurol Sci 2005;233:3–13.

52. Hires SA, Zhu Y, Tsien RY. Optical measurement of synaptic glutamate spillover and reuptake by linker optimized glutamate-sensitive fluorescent reporters. Proc Natl Acad Sci U S A 2008; 105:4411–4416.

53. Siffrin V, Radbruch H, Glumm R, et al. In vivo imaging of partially reversible th17 cell-induced neuronal dysfunction in the course of encephalomyelitis. Immunity 2010;33:424–436.

54. Hertz L, Peng L, Dienel GA. Energy metabolism in astrocytes: high rate of oxidative metabolism and spatiotemporal dependence on glycolysis/glycogenolysis. J Cereb Blood Flow Metab 2007;27:219–249.

55. Bélanger M, Allaman I, Magistretti PJ. Brain energy metabolism: focus on astrocyte-neuron metabolic cooperation. Cell Metab 2011;14:724–738.

56. Magistretti PJ. Neuron-glia metabolic coupling and plasticity. J Exp Biol 2006;209(pt 12):2304–2311.

57. Desagher S, Glowinski J, Premont J. Astrocytes protect neurons from hydrogen peroxide toxicity. J Neurosci 1996;16:2553–2562.

58. Swanson RA, Ying W, Kauppinen TM. Astrocyte influences on ischemic neuronal death. Curr Mol Med 2004;4:193–205.

59. Trendelenburg G, Dirnagl U. Neuroprotective role of astrocytes in cerebral ischemia: focus on ischemic preconditioning. Glia 2005; 50:307–320.

60. Papadopoulos MC, Verkman AS. Aquaporin water channels in the nervous system. Nat Rev Neurosci 2013;14:265–277.

61. Ochs S, Pourmand R, Jersild RA, Friedman RN. The origin and nature of beading: a reversible transformation of the shape of nerve fibers. Prog Neurobiol 1997;52:391–426.

62. Ratelade J, Verkman AS. Inhibitor(s) of the classical complement pathway in mouse serum limit the utility of mice as experimental models of neuromyelitis optica. Mol Immunol 2014;62:104–113.

63. Kowarik MC, Dzieciatkowska M, Wemlinger S, et al. The cerebrospinal fluid immunoglobulin transcriptome and proteome in neuromyelitis optica reveals central nervous system-specific B cell populations. J Neuroinflammation 2015;12:19.